# Thesis

Ekaterina Avdeeva

University of Nebraska-Lincoln, USA

November 4, 2016

**Abstract**

This paper reviews

# Contents

# 1  Introduction

Elementary particle physics describes our world in terms of its smallest constituents, fundamental particles, and their interactions. Going from larger to smaller scales, substances around us consist of molecules, molecules consist of atoms, in an atom, there is a nucleus made of neutrons and protons and some number of electrons occupying their orbits around the nucleus. Protons and neutrons have a structure while an electron is not known to have any structure, therefore, an electron is an example of a particle which is considered to be fundamental.

Interactions of elementary particles are described by quantum field theories which incorporate principles of the quantum mechanics and the special theory of relativity. The set of such theories, including quantum elecrtrodynamics (QED), quantum chromodynamics (QCD) and the theory of weak interactions is called the Standard Model (SM). It has been proven to be an accurate description of interactions of elementary particles observed by now.

However, there are several experimental observations which are not described by the SM such as gravity, dark matter, dark energy, matter/antimatter asymmetry and others. Therefore, the SM is not the complete theory of particle interactions. There are several SM extensions offered by theorists as well as radically new theories waiting for the experimental confirmation or disproof.

Some SM extensions and new theories predict the existence of heavy particles mass of which possibly lies beyond experimentally reachable energies. The search of these particles is one of the prioritized directions in particle physics. For such searches we need to reach higher energies than those which were probed before. One source of highly energetic elementary particles is cosmic rays. The most energetic particles ever observed came from this source. However, cosmic rays are totally uncontrollable and such highly energetic particles are rare. If we want to produce a large number of particles at certain energies, we need to use a particle accelerator. A large number of events at certain energy allows experimentalists to perform a statistical analysis and increase the probability of finding a new particle if it exists in the given energy range.

Symmetric colliding beams is the most effective way to produce as heavy particles as possible given the energies of the colliding particles. The Large Hadron Collider (LHC) is such a collider with the highest energy in the world ever built. It can produce the most massive particles to probe physics beyond the SM. It collides two proton beams with the several TeV of energy each. The design center-of-mass energy of LHC is 14 TeV but it also probes several lower energy points and may go higher.

Compact Muon Solenoid (CMS) is one of two general-purpose detectors at the LHC. It is placed at one of six collision points. CMS has a wide physics program including searches for the beyond SM (BSM) physics as well as the precision measurements of the SM parameters themselves.

In this dissertation the analysis of $pp \rightarrow W\gamma + X$ processes using leptonic decays of $W \rightarrow \ell\nu$ where $\ell = e, \mu$ is reported. The $W\gamma$ productions with leptonic $W$ decays can go through one of the following three processes: initial state radiation where a photon is produced from one of the incoming partons, final state radiation where a photon is radiated off the charged lepton from the $W$ boson decay, and finally when a photon is produced via the triple gauge coupling (TGC) where a photon is emitted from the $W$ boson.

To search for the deviations from the SM, one would search for an anomalous TGC which would be indicated by the enhance of the TGC production over the SM prediction.

The total and the differential cross section with respect to the photon transverse momentum $(P_T^\gamma)$ has been measured. The $P_T^\gamma$ is sensitive to the potential anomalous TGC (aTGC) in the high $P_T^\gamma$ region. The disagreement between the measured and theoretically predicted differential cross section at the higher $P_T^\gamma$ end would be an indication of the possible presence of the aTGC.

The rest of this chapter gives general introductory information about the SM while chapter 2 concentrates on the theory of the SM and BSM $W\gamma$ production and also discusses previous measurements of this process. Chapter 3 describes LHC and CMS in more details. Chapter 4 explaines on specific aspect of the CMS operation which is the tracker alignment. Finally, chapter 5 describes the details of the measurement of this dissertation and reports the results.

## 1.1 Fundamental Particles and Interactions

The SM describes interactions of elementary particles. There are four fundamental interactions: electromagnetic, strong, weak and gravitational. The gravity is not included into the SM but its effect on particles is negligible compared to the other forces which makes it possible to develop a theory of the particle physics and conduct experiments even without having the gravity included into the model.

All fundamental elementary particles in the SM can be split into three categories by their spins. There are fermions which possess spin s=1/2, there are gauge bosons which are also called force mediators are vector particles (s=1) and there is the Higgs boson which is a scalar particle (s=0).

The fermions are arranged into three generations, each generation consists of a quark with charge Q=+2/3(up, charm, and top quarks), a quark with Q=−1/3 (down, strange, and bottom quarks), a charged lepton with Q=−1 (electron, muon, and tau-lepton) and a neutrino (electron, muon, and tau neutrinos) which is electrically neutral. Each quark can carry any of three colors: red, blue, or green. Additionally, each fermion has its antiparticle. Therefore, the total number of fundamental fermions is $(6(leptons) + 6(quarks) \cdot 3(colors)) \cdot 2(to\ include\ antiparticles) = 48$.

Corresponding particles in different generations have the same charges, spins and interaction properties but masses of particles increase with a generation. These mass differences lead to different decay properties because a particle A can decay to particles B and C only if the mass of A $m_A > m_B + m_C$. Thus, an electron is a stable particle, a muon decays as $\mu^- \to e^- + \bar{\nu}_e + \nu_\mu$, a tau-lepton, as the heaviest charged lepton, has the largest number of decay channels: $\tau^- \to \mu^- + \bar{\nu}_\mu + \nu_\tau$, $\tau^- \to e^- + \bar{\nu}_e + \nu_\tau$, $\tau^- \to \nu_\tau +$ quarks.

In addition to fermions, the SM includes gauge bosons which are mediators for the SM interactions. A photon is a mediator for the electromagnetic interactions, a gluon is a mediator for the strong interactions, and $W^\pm$ and $Z^0$ bosons are mediators for the weak interactions. $W^\pm$ and $Z^0$ bosons are massive while a photon and a gluon are massless particles.

The last SM particle is the Higgs boson. The Higgs boson is a scalar neutral particle which is playing a critical role in the electroweak symmetry breaking. The Higgs mechanism describes how $W$ and $Z$ bosons become massive particles.

All the particles are summarized in Fig. 1. These and only these fundamental particles and their antiparticles have been discovered by now. However, there are many composite particles which are called hadrons. Hadrons can consist of three quarks (baryons), quark and antiquark (meson), or three antiquarks (antibaryons). Hadrons always possess an integer charge.

Most of the particles are short-lived and decay within microseconds. The only stable particles are protons and antiprotons, electrons and positrons, neutrinos and antineutrinos, photons, and, in some sense, gluons. However, if a particle cannot decay, it does not mean that it would live forever. There are many different kinds of reactions in which particles can disappear. Antiprotons and positrons would immediately annihilate with protons and electrons, photons can be absorbed by charged particles, electrons and protons can scatter to produce neutrons and neutrinos and many other reactions are possible.

In this dissertation a process is studied where quark and antiquark interact to produce a $W$ boson which then decay as $W^\pm \to e^\pm \nu_e(\bar{\nu}_e)$ or $W^\pm \to \mu^\pm \nu_\mu(\bar{\nu}_\mu)$. A photon is radiated off a quark or antiquark, a charged lepton or a $W$ boson. The most interesting mechanism out of three is a radiation from a $W$ boson because this is the triple gauge coupling where we potentially can have a new physics. Therefore, the focus of this study is an interaction between a photon and a $W$ boson however many other SM particles are relevant too. Thus, a charged lepton and a neutrino appear as the final state particles, a quark and an antiquark appear as initial state

particles and all fundamental particles except the Higgs boson participate in various background processes. Subsections 1.2-1.4, chapter 2 and [1] describe particle interactions in more details.
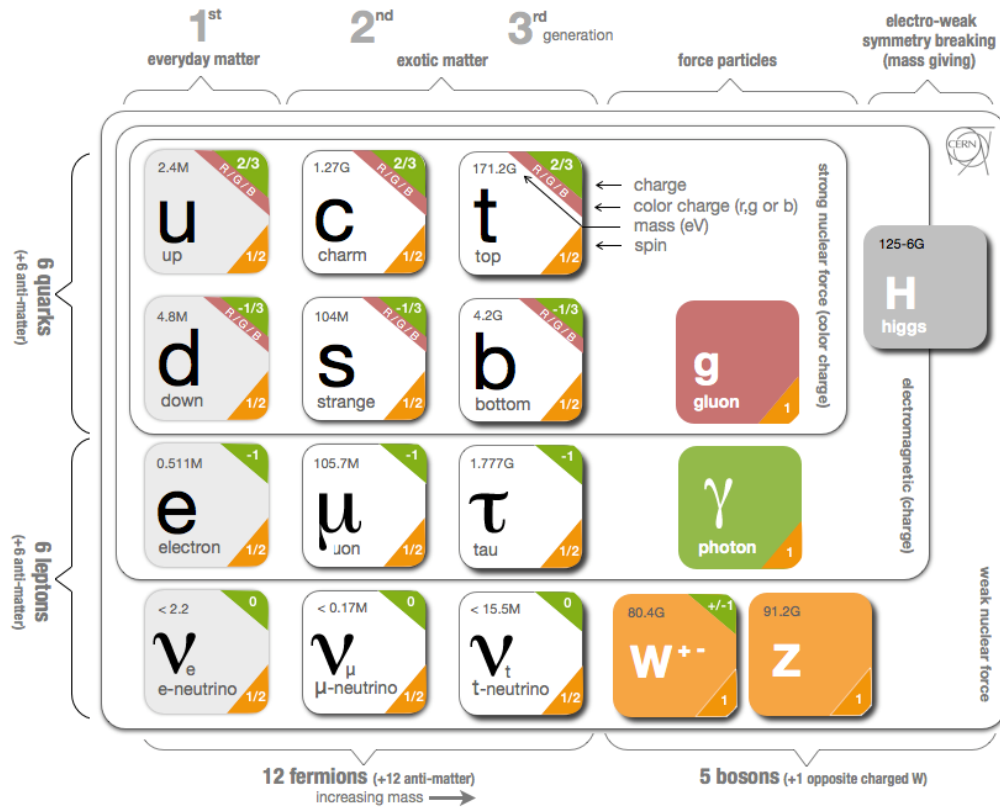


Figure 1: Standard Model Particles and Interations. Source of the figure: [2].

## 1.2 Electroweak Interactions

All electrically charged particles participate in electromagnetic interactions. All electromagnetic interactions are mediated by a photon, a spin-one electrically neutral massless particle, and can be reduced to one elementary process (Fig. 2, left). This process represents an electron radiating or absorbing a photon. Although an electron is drawn in this figure, it can be any other charged particle as well. Such elementary process itself is forbidden by the energy conservation law but this element is a base of actual process (for example, Fig. 2, middle and right). Such graphical representations of the particle physics processes are called Feynman diagrams.
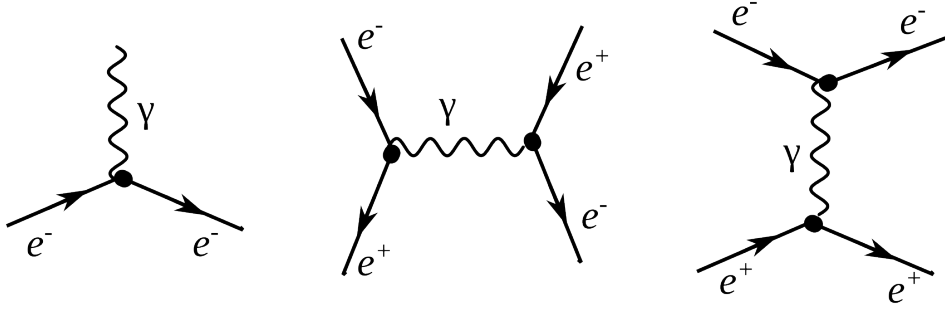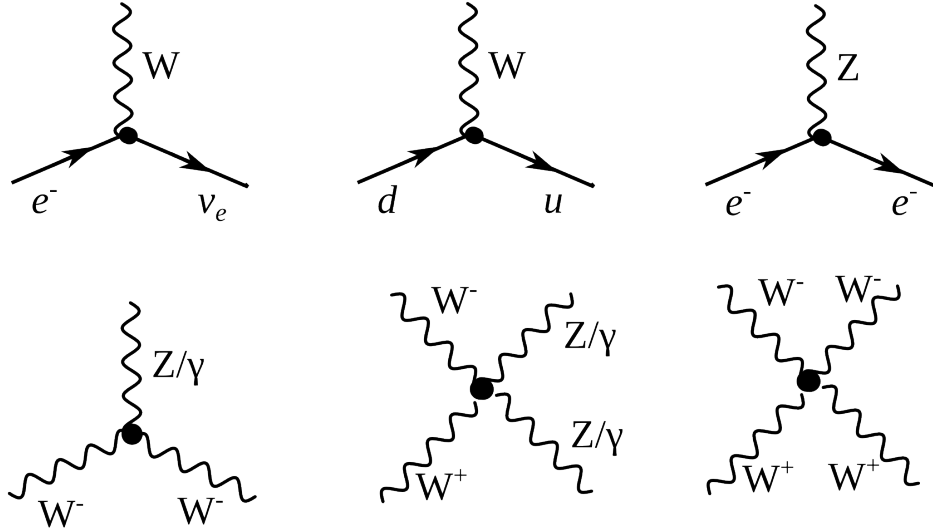


Figure 2: Electromagnetic interations



Figure 3: Weak elementary processes and gauge couplings

As for the weak interactions, there are two kinds of them: neutral (mediated by a $Z$ boson) and charged (mediated by a $W^{\pm}$ boson). Elementary processes with $W$ and $Z$ bosons are shown in Fig. 3. Because the electric charge must be conserved at any vertex, a particle radiating

or absorbing a $W$ boson converts to a different particle. Thus, a charged lepton converts to a neutrino (or vice versa) as shown in Fig. 3, top left. Each lepton carries a lepton flavor number (Tab. 1). A lepton flavor number is conserved in any interaction, thus an electron radiating a $W$ boson always converts to an electron neutrino, a muon converts to a muon neutrino etc.

Table 1: Lepton Flavor Number

| particles | $L_e$ | $L_\mu$ | $L_\tau$ |
|-----------|-------|---------|----------|
| $e^-, \nu_e$ | +1 | 0 | 0 |
| $e^+, \bar{\nu}_e$ | -1 | 0 | 0 |
| $\mu^-, \nu_\mu$ | 0 | +1 | 0 |
| $\mu^+, \bar{\nu}_\mu$ | 0 | -1 | 0 |
| $\tau^-, \nu_\tau$ | 0 | 0 | +1 |
| $\tau^+, \bar{\nu}_\tau$ | 0 | 0 | -1 |

From top middle diagram in Fig. 3 we see that if a quark with Q=$-1/3$ enters, then a quark with Q=$+2/3$ escapes and, therefore, the flavor of the quark is changed. The charged weak interaction is the only interaction which changes a quark flavor. The probability of each of three quarks with Q=$+2/3$ to be born is determined by the Cabibbo Kobayashi Maskawa matrix and is the highest for the quark of the same generation as an initial state quark. In this particular case, $d$ is the initial state quark and $u$ has the highest probability to be produced after an interaction with a $W$ boson but $c$ and $t$ can also be produced if there is enough energy.

An elementary process of a neutral weak interaction is an emission of a $Z$ boson off a fermion line (right top diagram in Fig. 3). An electron is shown here as an example however it could also be any lepton, antilepton, quark or antiquark. Diagrams with a $Z$ boson are very similar to ones with a photon except a photon can only be radiated off a charged particle but a $Z$ boson can also be radiated off a neutrino or antineutrino.

The bottom diagrams in Fig. 3 are gauge bosons coupling diagrams including self-coupling of a $W$ boson, its interaction with a $Z$ boson and its electromagnetic radiation of a photon. $WWZ$, $WW\gamma$, $WWZZ$, $WWZ\gamma$, $WW\gamma\gamma$ and $WWWW$ vertices are all possible in the SM.

Electromagnetic and weak interactions are unified by the electroweak Glashow-Weinberg-Salam (GWS) theory which is based on $SU(2) \times U(1)$ symmetry. $SU(2)$ is the symmetry of weak isospin which generates three bosons: $W^1$, $W^2$ and $W^3$. $U(1)$ is the symmetry of the weak hypercharge and generate one neutral boson $B$. $W^1$ and $W^2$ are mixed to create $W^+$ and $W^-$ mediators while $W^3$ and $B$ are mixed to create a $Z$ boson and a photon. Therefore, the GWS theory considers electromagnetic and weak forces as different manifestations of the electroweak force.

However, weak interactions are mediated by heavy bosons ($M_W = 80$ GeV, $M_Z = 91$ GeV) while electromagnetic interactions are mediated by a massless photon, thus, the electroweak symmetry is broken. To explain this phenomenon, the Higgs mechanism was introduced. The mechanism predicted an existence of an additional boson: the Higgs boson. The Higgs boson was a missing piece of the SM for many years and was finally discovered in 2012 at LHC by ATLAS and CMS collaborations through the processes shown in Fig.4 [3], [4].

The measurement in this dissertation is an electroweak measurement because the process involves a $W$ boson. It includes an interaction of a $W$ boson with leptons and quarks as well as the triple gauge coupling $WW\gamma$. Thus, the measurement is a good test of the SM electroweak theory.
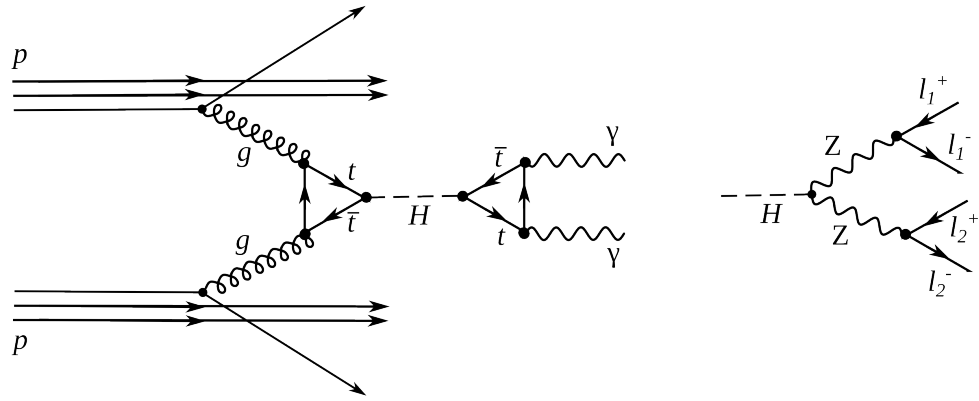
Figure 4: The Higgs boson production and decay
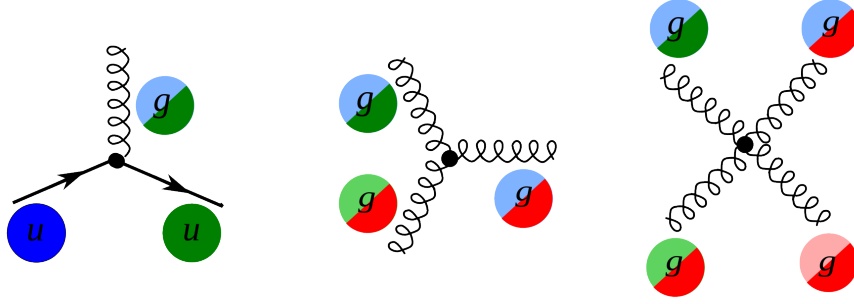
205

## 1.3 Strong Interactions



Figure 5: Elementary processes of strong interations

The third fundamental force after the electromagnetic and weak ones is the strong force. The strong force is responsible for glueing protons and neutrons together in the nuclei as well as for forming protons and neutrons themselves. The strong interactions occur by exchanging gluons which are spin-one massless electrically neutral particles.

The elementary strong processes are shown in Fig. 5. There are three elementary processes: $qqg$, $ggg$ and $gggg$, all are involving particles with color charges. Thus, gluons couple to quarks and self-couple. Color charges must be conserved at each elementary process of the strong interaction. Because quarks can possess three colors, there are eight types of gluons to cover all possible color exchanges.

The coupling constant of the strong interaction depends on a distance between interacting particles: it becomes larger as the distance becomes larger. This property leads to two consequences specific to the strong force: the confinement and the asymptotic freedom.

The asymptotic freedom means that when quarks are very close to each other they almost do not interact with each other and therefore they are free. The confinement is the property of quarks to always stay in the color neutral combinations (hadrons), it forbids the existence of free quarks. A combination becomes color neutral when there is the same amount of color and anticolor or if there is the same amount of each of the three colors. Thus, mesons are comprised of a quark and an antiquark with the opposite color charges, and baryons are comprised of three quarks: red, green and blue one. Examples of baryons include such well-known particles as a proton and a neutron are baryons.

The strong interactions can be described by the QCD which is a quantum field theory invariant under SU(3) color transformations. When the distance between quarks is small which corresponds to high energy, and thus the coupling constant $\alpha_s \ll 1$ is small, the perturbative approach can be used to compute observables.

The W$\gamma$ process being measured in this dissertation is not intended to test QCD, but a good understanding of QCD is essential for performing this measurement because the QCD corrections to the Feynman diagrams of the process are large and has to be taken into account in producing simulation. Possible QCD corrections include quark-gluon loops at any of three quark lines as well as exchanges of gluons between different quark lines. In addition, QCD describes the dynamics of quarks and gluons within colliding protons and predicts probabilities of one or another quark-antiquark pair to interact. Physics of proton-proton collisions is discussed in the subsection 1.4.

## 1.4 Physcis of Proton-Proton Collisions

At LHC two protons are collided. The LHC energy is so high that a proton behaves as a complex structure. A proton is a baryon, it consists of three quarks: $uud$. These three quarks are called valence quarks. They interact with each other by exchanging gluons which produce virtual $q\bar{q}$ pairs (Fig. 6). Such quarks are called sea quarks.

Any parton from one proton can interact with any parton from another proton. Probabilities $f_i(x, Q^2)$ of any particular constituent $i$ to interact are described partially by QCD and partially by experimental measurements and depend on the momentum transfer $Q$ and the momentum fraction of a specific parton $x$. These probabilities are called parton distribution functions (PDFs).
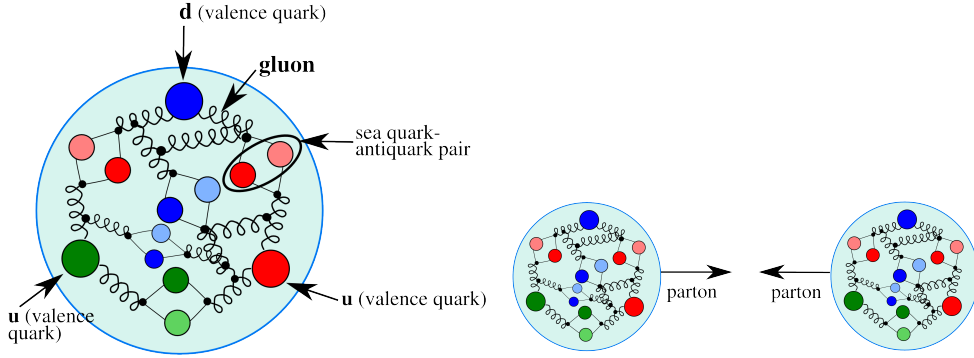


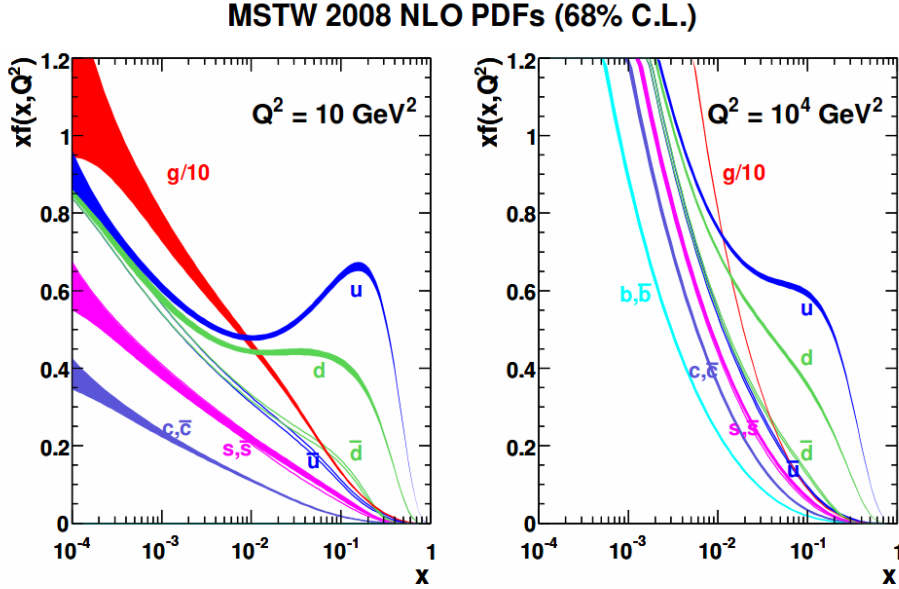Figure 6: The proton structure (left) and the proton-proton collision (right).



Figure 7: Martin-Stirling-Thorne-Watt parton distribution functions [5].

For large $Q^2$ and $x$ gluon-gluon interactions have the largest probabilities to occur (Fig. 7).

However, gluons do not couple directly to a $W$ boson, thus, in the $W\gamma$ measurement we are mostly interested in quark-antiquark pairs which would have a total charge corresponding to the charge of a $W$ boson ($\pm 1$). Since we have $u$ and $d$ as valence quarks and we know that the probability to couple to the same generation quark in charged weak interactions is the highest, most of the $W$ bosons are created by $u\bar{d}$ and $d\bar{u}$ pairs however other $q\bar{q}'$ combinations with the total charges of $\pm 1$ are also possible. The antiquarks come from virtual $q\bar{q}$ pairs inside of each proton.

As we look for events containing $W\gamma$ we also have other events mimicking our process. Such background events can be produced by any pair of partons.

## 1.5  Open Questions of the Standard Model

While the SM is an accurate description of all particle physics experimental results, there are certain phenomena which are not included into the SM. In this subsection we discuss some of them.

The gravitational interactions do not fit into the SM. It is the open question whether the quantum theory of gravity is possible and whether there is a mediator of the gravitational interactions. Also, it is not known why the gravitational force is so much weaker than any other force. One possible explanation comes from a theory which predicts extra spatial dimensions beyond the three we are dealing with (e.g. the string theory). In this case, it is possible that the gravitational force is shared with other dimensions and that is why the fraction available in our three dimensions is that small.

Another mystery of the Universe is its composition: it is known from the studies of the gravitational effects that our Universe consists of dark energy by 70%, of dark matter by 26% and of baryon matter only by 4%. The dark energy resists the gravitational attraction and accelerates the expansion of the Universe, and is not detectable by any effects except gravitational. The understanding of the dark energy is a question of the general relativity rather than the particle physics. The dark matter however likely consists of particles and therefore is a subject of the particle physics. It does not radiate and that is why it cannot be detected by telescopes. The nature of the dark matter is not known but its constituents must be very stable to remain since the Big Bang. The theory of the supersymmetry which is unifying fundamental particles and mediators predicts many of new heavy particles and the lightest supersymmetric particle, the neutralino, is a good candidate for the dark matter.

One more open question is the reason for the matter/antimatter asymmetry. The matter and antimatter should have been created in the same amount at the moment of the Big Bang. Then most of it has annihilated but because of asymmetry, there was more matter than antimatter which led to the state of the Universe we observe now. There is a phenomenon of the CP-violation in weak interactions observed and described that predicts the asymmetry at a certain level. However, the effect of the CP-violation is not large enough to account for the observed amount of the matter and, therefore, the total matter/antimatter asymmetry remains unexplained.

The measurement of the photon transverse momentum spectrum ($P_T^\gamma$) of the $W\gamma$ process has a goal to both test the SM and search for the BSM physics. The low $P_T^\gamma$ region is not expected to be affected by any new physics and must agree well with the SM predictions while the high $P_T^\gamma$ region may indicate an existence of a new physics if there is an enhance over the SM predictions. The enhance would be an indirect evidence of the BSM particles like supersymmetric particles, additional gauge bosons or higher generation fermions. More theoretical details about the SM descriprion of $W\gamma$ process as well as the possible BSM physics are given in the chapter 2.

# 2 $W\gamma$ Production Theory and Former Experimental Results

## 2.1 Electroweak Theory of the Standard Model

To develop a quantum field theory, we start with the Lagrangian of free fermions. Then we require a local invariance with respect to a certain transformation which corresponds to a conservation of a physical quantity. The requirement of the local invariance introduces a new vector field (or several fields) which is a mediator of an interaction conserving the physical quantity. Then, to make the vector field a physical boson, invariant term for the kinetic energy of the boson is introduced. Such approach allows us to derive the Lagrangian which is locally invariant with respect to a certain gauge transformation and contains interacting fermions as well as mediators.

The SM is a quantum field theory invariant under the local $SU(3)_C \times SU(2)_L \times U(1)_Y$ transformation [6].

$SU(3)_C$ stands for color transformations and, therefore, the $SU(3)_C$-invariant Lagrangian describes QCD: color interactions of quarks and antiquarks. The requirement to satisfy the gauge invariance generates eight massless gluons, and the non-abelian nature of the $SU(3)$ group generates self-interactions of gluons including three-gluon and four-gluon vertices.

The Lagrangian based on the $SU(2)_L \times U(1)_Y$ symmetry where $L$ stands for left-handed fermions ([1], Ch. 9) and $Y$ stands for a weak hypercharge describes unified theory of electroweak interactions. The requirement of the local gauge invariant generates four massless vector bosons which are mediators of electromagnetic and weak interactions. The non-abelian structure of $SU(2)$ group introduces gauge boson couplings just like self-interactions of gluons appear in QCD.

Mass terms for the vector bosons would violate the gauge invariance of the electroweak Lagrangian, however it is experimentally known that mediators of weak interactions are heavy particles with masses $M_W = 80$ GeV and $M_Z = 91$ GeV. That means that electroweak symmetry is spontaneously broken. QED symmetry group $U(1)$ remains unbroken because a photon is massless.

The mechanism of the Spontaneous Symmetry Breaking and the appearance of the mass terms for $W$ and $Z$ boson can be described by introducing an additional particle into the SM: a Higgs boson ($H$). The Higgs boson couples to $W$ and $Z$ bosons generating their masses while a photon does not couple to the Higgs boson remaining a massless particle and keeping $U(1)_{QED}$ symmetry unbroken.

The measurement in this dissertation provides a test for the electroweak sector of the SM, thus we will repeat here the derivations from the Lagrangians of free particles to the accommodation of the electroweak gauge bosons including their self-couplings to explain better what model is tested.

It is experimentally known that dynamics of weak interactions depends on particle's helicity ([1], Ch. 4.4.1). In particular, a $W$ boson couples to left-handed fermions and right-handed antifermions only. A $Z$ boson couples to both left-handed and right-handed charged fermions and antifermions but only to left-handed neutrinos and right-handed antineutrinos.

Given different properties of left-handed and right-handed fermions, they are treated differently by the electroweak theory. $SU(2)$ doublets are introduced for the wave functions of left-handed fermions while $SU(2)$ singlets are introduced for the wave functions of right-handed fermions. Eq. 1 and Eq. 2 show wave functions for the first generation fermions. Wave functions for the other two generations are constructed the same way.

$$\psi_1(x) = \begin{pmatrix} u \\ d' \end{pmatrix}_L, \ \psi_2(x) = u_R, \ \psi_3(x) = d'_R. \tag{1}$$

$$\psi_1(x) = \begin{pmatrix} \nu_e \\ e^- \end{pmatrix}_L, \ \psi_2(x) = \nu_{eR}, \ \psi_3(x) = e_R^-. \tag{2}$$

The state $d'$ is a mixture of $d$, $c$ and $b$ quark's wave functions and is determined by the quark mixing matrix which is also called Cabbibo-Kobayashi-Maskawa matrix [6]:

$$\begin{pmatrix} d' \\ c' \\ b' \end{pmatrix} = V \begin{pmatrix} d \\ c \\ b \end{pmatrix} \tag{3}$$

To derive the unified electroweak Lagrangian, we start with the free fermion terms:

$$L_0 = \sum_{j=1}^3 i\bar{\psi}_j(x)\gamma^\mu \partial_\mu \psi_j(x), \tag{4}$$

where $\gamma^\mu$ are Dirac matrices ([1], Ch. 7.1) and $\psi_j(x)$ are wave functions determined by Eq. 1 and Eq. 2.

The wave function $\psi_1$ changes under the $SU(2)_L \times U(1)_Y$ transformations in the following way:

$$\psi_1(x) \rightarrow e^{iy_1\beta} U_L \psi_1(x) \tag{5}$$

The wave functions $\psi_{(2,3)}(x)$ are singlets of $SU(2)_L$ and are affected only by $U(1)$ transformations:

$$\psi_{(2,3)}(x) \rightarrow e^{iy_{(2,3)}\beta} \psi_{(2,3)}(x) \tag{6}$$

The transformation $U_L \equiv e^{i\sigma_i\alpha_i/2}$ where $\sigma_i$ are Pauli matrices ([1], Ch. 4.2.2). Phases $\alpha_i(x)$ and $\beta(x)$ are arbitrary functions, $y_{(1,2,3)}$ are hypercharges which are named analogous to electric charges in QED.

In order to satisfy the local $SU(2)_L \times U(1)_Y$ invariance, partial derivatives in Eq. 4 have to be substituted with covariant derivatives:

$$D_\mu \psi_1(x) = [\partial_\mu - ig\tilde{W}_\mu(x) - ig'y_1 B_\mu(x)]\psi_1(x) \tag{7}$$

$$D_\mu \psi_{(2,3)}(x) = [\partial_\mu - ig'y_{(2,3)} B_\mu(x)]\psi_{(2,3)}(x) \tag{8}$$

where $g$, $g'$ are arbitrary constants,

$$\tilde{W}_\mu(x) \equiv \frac{\sigma_i}{2} W_\mu^i(x) = \frac{1}{\sqrt{2}} \begin{pmatrix} \sqrt{2}W_\mu^3 & (W_\mu^1 - iW_\mu^2)/\sqrt{2} \\ (W_\mu^1 + iW_\mu^2)/\sqrt{2} & -W_\mu^3 \end{pmatrix}, \tag{9}$$

$B_\mu$, $W_\mu^1$, $W_\mu^2$, $W_\mu^3$ are four vector bosons that arise from the requirement of the Lagrangian to be invariant under local $SU(2)_L \times U(1)$ transformations.

The Lagrangian becomes:

$$L_0 \rightarrow L = \sum_{j=1}^3 i\bar{\psi}_j(x)\gamma^\mu D_\mu \psi_j(x) \tag{10}$$

To make new vector bosons physical fields it is necessary to add terms for their kinetic energies:

$$L_{KIN} = -\frac{1}{4}B_{\mu\nu}B^{\mu\nu} - \frac{1}{4}W^i_{\mu\nu}W^{\mu\nu}_i \tag{11}$$

where $B_{\mu\nu} \equiv \partial_\mu B_\nu - \partial_\nu B_\mu$, $W^i_{\mu\nu} \equiv \partial_\mu W^i_\nu - \partial_\nu W^i_\mu + g\epsilon^{ijk}W^j_\mu W^k_\nu$

Off-diagonal terms of $\tilde{W}_\mu$ are wave functions of charged vector bosons $W^\pm = (W^1_\mu \mp iW^2_\mu)/\sqrt{2}$ while $W^3_\mu$ and $B_\mu$ are neutral fields which are mixtures of a $Z$ boson and a photon determined by:

$$\begin{pmatrix} W^3_\mu \\ B_\mu \end{pmatrix} \equiv \begin{pmatrix} \cos\theta_W & \sin\theta_W \\ -\sin\theta_W & \cos\theta_W \end{pmatrix} \begin{pmatrix} Z_\mu \\ A_\mu \end{pmatrix} \tag{12}$$

where $\theta_W$ is an electroweak mixing angle, $A_\mu$ is a photon field.

In order to be consistent with QED, terms involving $A_\mu$ in the electroweak Lagrangian must be equal to the corresponding terms in QED Lagrangian [6]:

$$L_{QED} = i\bar{\psi}(x)\gamma^\mu\partial_\mu\psi(x) - m\bar{\psi}(x)\psi(x) + qA_\mu(x)\bar{\psi}(x)\gamma^\mu\psi(x) - \frac{1}{4}F_{\mu\nu}(x)F^{\mu\nu}(x), \tag{13}$$

where $q$ is electric charge of $\psi(x)$ field, $F_{\mu\nu} \equiv \partial_\mu A_\nu - \partial_\nu A_\mu$.

This requirement relates $g$, $g'$, $\theta_W$ and $e$ as $g\sin\theta_W = g'\cos\theta_W = e$ and provides expression for weak hypercharges: $y = q - t_3$, where $q$ is the electric charge and $t_3$ is a $z$-component of the weak isospin. This gives $y_1 = 1/6$, $y_2 = 2/3$, and $y_3 = -1/3$ for quarks and $y_1 = -1/2$, $y_2 = 0$, and $y_3 = -1$ for leptons. A right-handed neutrino has a hypercharge of $y_2 = 0$. It also does not have an electric charge and, as a right-handed particle, cannot couple to a $W$ boson. Thus, a right-handed neutrino does not participate in any SM interaction.

Writing $\tilde{W}_\mu$ in Eq. 11 explicitly, we will get TGC and QGC coupling terms:

$$L_{TGC} = -\frac{g}{4}(\partial_\mu W^i_\nu - \partial_\nu W^i_\mu)\epsilon^{ijk}W^{\mu j}W^{\nu k} - \frac{g}{4}\epsilon^{ijk}W^j_\mu W^k_\nu(\partial^\mu W^{\nu i} - \partial^\nu W^{\mu i}) \tag{14}$$

$$L_{QGC} = -\frac{g^2}{4}\epsilon^{ijk}\epsilon^{ilm}W^j_\mu W^k_\nu W^{\mu l}W^{\nu m} \tag{15}$$

Substitute $W^i_\mu$ and $B_\mu$ in Eq. 14 and Eq. 15 with the wave functions of $W^\pm$, $Z$ and a photon:

$$B_\mu = -\sin\theta_W Z_\mu + \cos\theta_W A_\mu, \quad W^3_\mu = \cos\theta_W Z_\mu + \sin\theta_W A_\mu \tag{16}$$

$$W^1_\mu = \sqrt{2}(W^+ + W^-), \quad W^2_\mu = \sqrt{2}(W^- + W^+) \tag{17}$$

we will receive charged TGC Lagrangians in the form of Eq. 18:

$$L_{TGC} = L^{(1)}_{TGC} + L^{(2)}_{TGC}, \tag{18}$$

which involves $WWZ$ (Eq. 19) and $WW\gamma$ (Eq. 20) interactions:

$$L^{(1)}_{TGC} = -ie\cot\theta_W(W^{-\mu\nu}W^+_\mu Z_\nu - W^{+\mu\nu}W^-_\mu Z_\nu + W^-_\mu W^+_\nu Z^{\mu\nu}), \tag{19}$$

$$L^{(2)}_{TGC} = -ie(W^{-\mu\nu}W^+_\mu A_\nu - W^{+\mu\nu}W^-_\mu A_\nu + W^-_\mu W^+_\nu A^{\mu\nu}), \tag{20}$$

and charged QGC Lagrangians in the form of Eq. 21:

$$L_{QGC} = L_{QGC}^{(1)} + L_{QGC}^{(2)} + L_{QGC}^{(3)} + L_{QGC}^{(4)} \tag{21}$$

which involves $WWWW$ (Eq. 22), $WWZZ$ (Eq. 23), $WWZ\gamma$ (Eq. 24), and $WW\gamma\gamma$ (Eq. 25) interactions:

$$L_{QGC}^{(1)} = -\frac{e^2}{2\sin^2\theta_W}(W_\mu^+ W^{-\mu} W_\nu^+ W^{-\nu} - W_\mu^+ W^{\mu+} W_\nu^- W^{-\nu}) \tag{22}$$

$$L_{QGC}^{(2)} = -e^2\cot^2\theta_W(W_\mu^+ W^{-\mu} Z_\nu Z^\nu - W_\mu^+ Z^\mu W_\nu^- Z^\nu) \tag{23}$$

$$L_{QGC}^{(3)} = -e^2\cot\theta_W(2W_\mu^+ W^{-\mu} Z_\nu A^\nu - W_\mu^+ Z^\mu W_\nu^- A^\nu - W_\mu^+ A^\mu W_\nu^- Z^\nu) \tag{24}$$

$$L_{QGC}^{(4)} = -e^2(W_\mu^+ W^{-\mu} A_\nu A^\nu - W_\mu^+ A^\mu W_\nu^- A^\nu) \tag{25}$$

In the measurement of this dissertation we probe $WW\gamma$ coupling.

The unified electroweak Lagrangian discussed above involves kinetic energy terms for fermions and gauge bosons as well as interactions of fermions with gauge bosons, TGC, and QGC. However, this Lagrangian does not contain any mass terms.

Because left-handed and right-handed wave functions transform differently under the electroweak symmetry, adding fermion mass terms of $\frac{1}{2}m_f^2\bar{\psi}\psi$ would violate the Lagrangian invariance and, therefore, fermion mass terms are forbidden by the $SU(2) \times U(1)$ symmetry requirement. Mass terms for gauge bosons also would violate the Lagrangian invariance just as a photon mass term $\frac{1}{2}m^2 A^\mu A_\mu$ would violate $U(1)$ invariance of $L_{QED}$ [1]. Therefore, Largangian $L$ in Eq. 10 contains massless particles only.

However, it is known from experiments that a $Z$ boson, a $W$ boson and fermions are massive particles and, therefore, our theory should accommodate their masses. To introduce masses into the electroweak Lagrangian, an $SU(2)_L$ doublet of complex scalar fields $\phi(x)$ is added to the Lagrangian:

$$\phi(x) \equiv \begin{pmatrix} \phi^{(+)}(x) \\ \phi^{(0)}(x) \end{pmatrix} \tag{26}$$

By selecting a special gauge of $\phi(x)$ it is possible to spontaneously break electroweak symmetry, generate a new scalar particle, a Higgs boson [6], and introduce mass terms for $W$ and $Z$ bosons and charged fermions through their couplings to the Higgs boson. The strength of the coupling constant is proportional to the square of the particle's mass, therefore, heavier particles are more likely to interact with $H$, and massless particles do not couple to $H$.

The mechanism of generating a fermion's mass involve both left-handed and right-handed components of the fermion. If our hypothesis that right-handed neutrinos do not exist is right, then the Higgs mechanism does not generate neutrino masses. However, from the experiments of neutrino oscillations, neutrinos are known to have masses even though they are orders of magnitude smaller than those of other fermions. Several hypotheses were offered to resolve this contradiction however at the moment the mechanism of neutrinos to acquire masses remain unknown [7].

In this dissertation, we study an electroweak process $W\gamma \to l\nu_l\gamma$, more specifically, probe TGC vertex $WW\gamma$ (Eq. 20). To do that, we are measuring a differential cross section with respect to the photon transverse momentum. The concept of the cross section in particle physics

462  is discussed in Chapter 2.2.

463

## 2.2 Cross Section and Luminosity

In this dissertation we are measuring the total and the differential cross section. The cross section in particle physics is the interaction probability per unit flux of incident particles [12]. It can be interpreted as area which must be crossed by an incident particle in order to interact with a scattering center, or, in case of a differential cross section, area $d\sigma$ within which an incident particle must appear to be scattered off by an angle $d\theta$ (Fig. 8). The relationship between $d\sigma$ and $d\theta$ gives us the expression for a differential cross section $d\sigma/d\theta$. Integrating over $d\theta$, one would get the total cross section $\sigma$.

In Fig. 8 an incident particle is the same as a final state particle, however in particle physics final state particles can differ from initial state particles, and we measure a differential cross section with respect to a parameter $X$ of the final state particle. Differentiating $\sigma$ by $X$ we get the expression for the differential cross section $d\sigma/dX$.
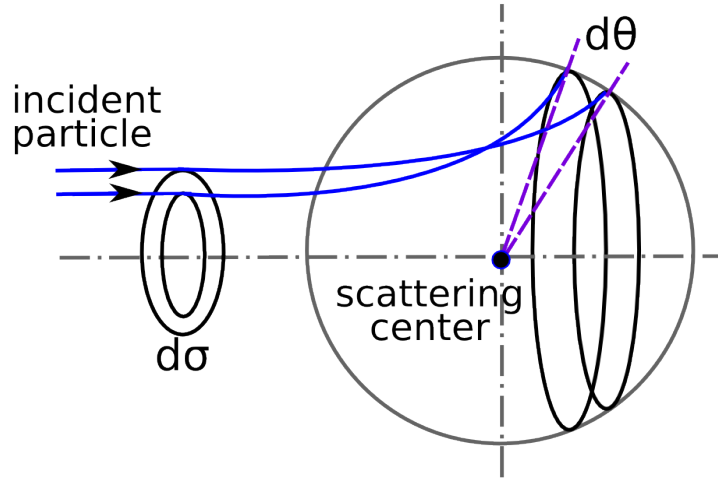


Figure 8: Illustration of the differential cross section concept in the classical case.

Referring to the Fig. 8, a number of particles passing through the area $\sigma$ per unit time is $N = L \cdot \sigma$, where $L$ is the flux of incident particles and is called luminosity. Therefore, the cross section $\sigma$ of a specific process can be determined from an experiment as $\sigma = N/L$.

A cross section also can be computed theoretically. The formula to compute a cross section is:

$$\sigma = \frac{W_{fi}}{L} N_{fs}, \tag{27}$$

where $W_{fi}$ is a transition probability between final and initial states of the system per unit volume, $L$ is the flux of initial particles, and $N_{fs}$ is the density of final states [8].

The formula of the cross section is called the Fermi's Golden Rule [1]. In case of the scattering of two particles to three final state particles $1 + 2 \rightarrow 3 + 4 + 5$, it takes the following form:

$$\sigma = \frac{1}{4\sqrt{(p_1 p_2)^2 - (m_1 m_2)^2}} \int |M|^2 (2\pi)^4 \delta^4(p_1 + p_2 - p_3 - p_4 - p_5) \prod_{j=3}^{5} \frac{1}{2\sqrt{\bar{p}_j^2 + m_j^2}} \frac{d^3\bar{p}_j}{(2\pi)^3}, \tag{28}$$

where $p_i$ are 4-momenta and $\bar{p}_i$ are three momenta of the initial state and the final state particles, $m_i$ are masses of particles. All available momenta of the final state particles is called the phase space.

The cross section of the hard scattering in proton-proton collisions $pp \rightarrow X + Y$ has two ingridients: PDFs and a partonic cross section $\sigma_{ab \rightarrow X}$. The partonic cross section is described by perturbative QCD while PDFs require non-perturbative computations and are determined, in part, from experiments (Fig. 7). According to the QCD factorization theorem [9]:

$$\sigma(pp \rightarrow X + Y) = \sum_{a,b} \int dx_a dx_b f_a(x_a, Q^2) f_b(x_b, Q^2) \sigma(ab \rightarrow X). \qquad (29)$$

In case of $W\gamma$ process, $X$ is $l\nu\gamma$, $ab$ are $q_i\bar{q}_j$ or $q_j\bar{q}_i$. $Q^2$ is the large momentum scale that characterizes hard scattering, $f_a$ and $f_b$ are PDFs, $x_a$ and $x_b$ are fractions of momenta of the partons.

## 2.3 Standard Model Wγ Production

A $W$ boson in proton-proton collisions can be produced in the processes $q\bar{q}' \to W$ where $q$ and $\bar{q}'$ are a quark and an antiquark which have a total charge of $+1$ if producing a $W^+$ boson or of $-1$ if producing a $W^-$ boson. The processes $u\bar{d} \to W^+$ and $d\bar{u} \to W^-$ are the most likely to occur because $u$ and $d$ are valence quarks in a proton. Antiquarks $\bar{d}$ and $\bar{u}$ come from sea $q\bar{q}$ pairs of the other proton.

A $W$ boson decays immediately after being created, and we do not detect the $W$ boson itself but its decay products. Decay modes of a $W$ boson include $W^{\pm} \to l^{\pm}\nu_l(\bar{\nu}_l)$ where $l^{\pm} = e^{\pm}$, $\mu^{\pm}$ or $\tau^{\pm}$ with branching fractions of 11% per a leptonic channel [7]. The rest 67% stands for various $W \to q\bar{q}'$ decays. In this dissertation we only consider $W^{\pm} \to \mu^{\pm}\nu_{\mu}(\bar{\nu}_{\mu})$ and $W^{\pm} \to e^{\pm}\nu_e(\bar{\nu}_e)$ as the cleanest channels.

A photon can be emitted from any charged particle of the process: a quark, an antiquark, a charged lepton or a $W$ boson (Fig. 9, top). A quark and an antiquark are initial state particles and, therefore, if one of them radiates a photon, we call such process the Initial State Radiation (ISR). A muon or an electron is a final state particle and if it radiates a photon, we call such process the Final State Radiation (FSR). Finally, a $W$ boson is a gauge boson and if it radiates a photon, the process has a vertex with three gauge bosons: $WW\gamma$, and we call such process the Triple Gauge Coupling (TGC).
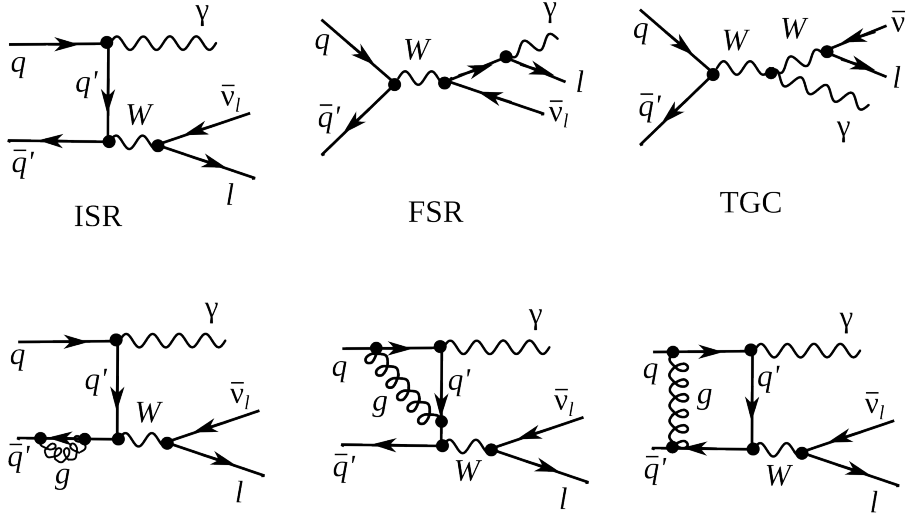


Figure 9: Feynman diagrams of Wγ production

The electroweak Lagrangian is described in Chapter 2.1. It is possible to derive equations of motion from the Lagrangian for any fields involved [1]. However, in a quantum field theory equations of motion cannot be solved exactly and, therefore, the perturbative approach is used if coupling constants are $g \ll 1$.

To represent the process graphically Feynman diagrams were invented. Also the diagrams can be used to calculate the process amplitude because they are determined by Lagrangian terms relevant to the process. There is infinite number of Feynman diagrams corresponding to any specific process and the total amplitude of the process is a sum of individual amplitudes of each diagram and it is not technically possible to take into account all of them. The perturbative approach

arranges all the diagrams by orders of contribution because each vertex is assigned a coupling constant and, therefore, the Feynman diagrams with fewer vertices would give a significantly larger contribution to the amplitude. In Fig. 9 we have examples of the Leading Order (LO) and the Next-to-Leading Order (NLO) Feynman diagrams (top and bottom diagrams respectively).

The NLO corrections shown in Fig. 9 are QCD corrections only which include gluon loops at the same quark line and exchange of a gluon between two different quark lines however QED and weak NLO diagrams are also possible. QED corrections mean radiations of extra photons by charged particles, exchange of photons between different charged particles or a photon can be radiated and absorbed by the same charged particle forming a loop. Similarly, weak corrections mean extra virtual $W$ or $Z$ bosons. But the QCD corrections are the largest.

The theoretical cross section in particle physics is important not only for analyzing the measurement result but also for producing the simulation which is then actively used while performing the measurement. The simulation consists of two parts: the generation of the process and the simulation of the particles paths through the detector. While the second one depends on the well-known properties of the particles and the detector configurations, the first part relies on the theory.

The most precise theoretical $W\gamma$ cross section available is the Next-to-Next-to-Leading Order (NNLO) cross section in QCD [14]. The effect of the NNLO correction ranges from 19% to 26% compared to the NLO cross section depending on the selection conditions. The contributions from the higher order corrections is estimated to be $\pm 4\%$. However, the NNLO theoretical result was published in 2015 only and there is still no simulation available based on that result. The simulation used in this analysis is LO + up to two hadronic jets simulation which found to give the same predictions as the NLO result.

In addition to the SM predictions, there are certain BSM theories which predict an enhancement of the contribution from the TGC diagram. The discussion of these BSM effects and how they affect the $W\gamma$ process takes place in Chapter 2.4.

## 2.4 Anomalous $W\gamma$ Production

Most BSM physics theories predict the existence of particles which are heavier than the discovered energy range. If their masses are not accessible even by the most energetic machines, the direct detection of such particles is not possible. However, they can contribute to the productions of lower energetic particles producing loops where such heavy particles would be off-shell. The loops would give additional contributions to the process amplitude and, therefore, there would be more events produced in the process than one can expect based on the SM predictions.

These effects can be probed by precision measurements of the SM processes. In the electroweak sector processes of such interest include diboson and triboson productions which can occur through triple gauge couplings and quartic gauge couplings.

Triple and quartic gauge couplings (QGC) are represented by vertices with three and four bosons (Fig. 10). As discussed in Chapter 2.1, charged TGC and QGC are possible at tree level in the SM while neutral TGC and QGC are not.
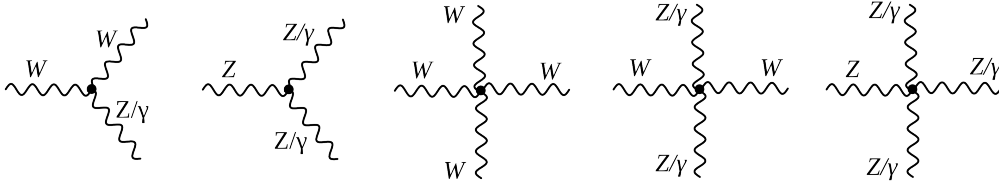
Figure 10: TGC and QGC vertices

To account for the effects from the potential loops of heavy particles, we introduce an effective Lagrangian with arbitrary values of coupling constants which can be shrunk to the SM Lagrangian if these constants would have their SM values. Such approach makes our searches model-independent because we do not specify which exactly particles form the loops but instead just check whether there is a deviation from the SM.

In $W\gamma$ measurement we can probe $WW\gamma$ vertex only. The most general Lorentz invariant Lagrangian of this vertex takes the following form [16]:

$$iL_{eff}^{WW\gamma} = iL_{eff(1)}^{WW\gamma} + iL_{eff(2)}^{WW\gamma} + iL_{eff(3)}^{WW\gamma} \tag{30}$$

$$iL_{eff(1)}^{WW\gamma} = e[g_1^\gamma A^\mu (W_{\mu\nu}^- W^{+\nu} - W_{\mu\nu}^+ W^{-\nu}) + \kappa_\gamma W_\mu^+ W_\nu^- A^{\mu\nu} + \frac{\lambda_\gamma}{m_W^2} A^{\mu\nu} W_\nu^{+\rho} W_{\rho\mu}^-] \tag{31}$$

$$iL_{eff(2)}^{WW\gamma} = e[ig_5^\gamma \epsilon_{\mu\nu\rho\sigma}((\partial^\rho W^{-\mu})W^{+\nu} - W^{-\mu}(\partial^\rho W^{+\nu}))V^\sigma + ig_4^\gamma W_\mu^- W_\nu^+ (\partial^\mu A^\nu + \partial^\nu A^\mu)] \tag{32}$$

$$iL_{eff(3)}^{WW\gamma} = e[\frac{\tilde{\kappa_\gamma}}{2} W_\mu^- W_\nu^+ \epsilon^{\mu\nu\rho\sigma} A_{\rho\sigma} - \frac{\tilde{\lambda_\gamma}}{2m_W^2} W_{\rho\mu}^- W_\nu^{+\mu} \epsilon^{\nu\rho\alpha\beta} A_{\alpha\beta}] \tag{33}$$

where $e$ is the absolute value of the electron charge, $A^\mu$ is the photon field, $W^{\pm\mu}$ are fileds of $W^\pm$ bosons, $W_{\mu\nu} = \partial_\mu W_\nu - \partial_\nu W_\mu$, $A_{\mu\nu} = \partial_\mu A_\nu - \partial_\nu A_\mu$, $m_W$ is the mass of a $W$ boson, $g_1^\gamma$, $\kappa_\gamma$, $\lambda_\gamma$, $g_5^\gamma$, $g_4^\gamma$, $\tilde{\kappa_\gamma}$, and $\tilde{\lambda_\gamma}$ are constants.

Despite there are 7 constants in the extended Lagrangian, only $\lambda_\gamma$ and $\kappa_\gamma$ are considered in the aTGC searches. The rest of the constants are fixed to their SM values based on various considerations. Thus, $g_1^\gamma = 1$ and $g_5^\gamma = 0$ are fixed to obey the electromagnetic gauge invariance for the on-shell photons. The non-zero value of $g_5^\gamma$ also violates C and P conservations, and non-zero values of $g_4^\gamma$, $\tilde{\kappa_\gamma}$, $\tilde{\lambda_\gamma}$ violate the CP conservation law. Such violation parametrizations are not considered in charged TGC measurements now but might get considered in the future.

The presence of aTGC would have larger effects at high energy scales. Fig. 11 shows these effect in $P_T^\gamma$ spectrum of 7 TeV $W\gamma \to \mu\nu\gamma$ measurement. Fig. 12 shows the examples of these effects in $m_{ll}$ spectrum in 8 TeV $WW \to l\nu l\nu$ measurement (left) and $P_T^\gamma$ spectrum in 7 TeV $Z\gamma \to \nu\nu\gamma$ measurement (right). It is seen on the plots that aTGC spectrum at low $m_{ll}$ or low $P_T^\gamma$ coincides with the SM prediction but for higher $m_{ll}$ or $P_T^\gamma$ the disagreement becomes more significant.
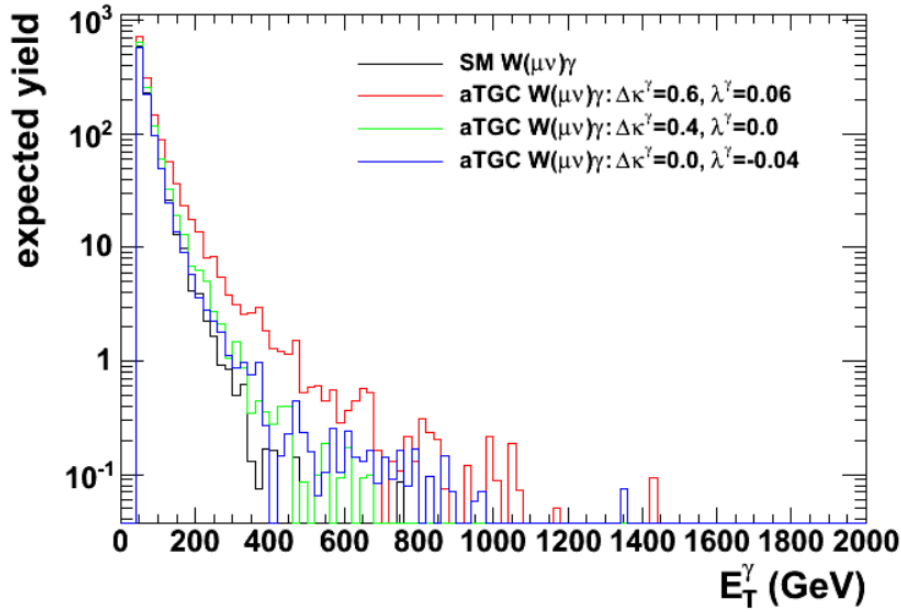


Figure 11: Distributions of $P_T^\gamma$ of simulated $W\gamma \to \mu\nu\gamma$ events with different values of aTGC constants at LHC energy of $\sqrt{s} = 7$ TeV. Source of figure: [17].
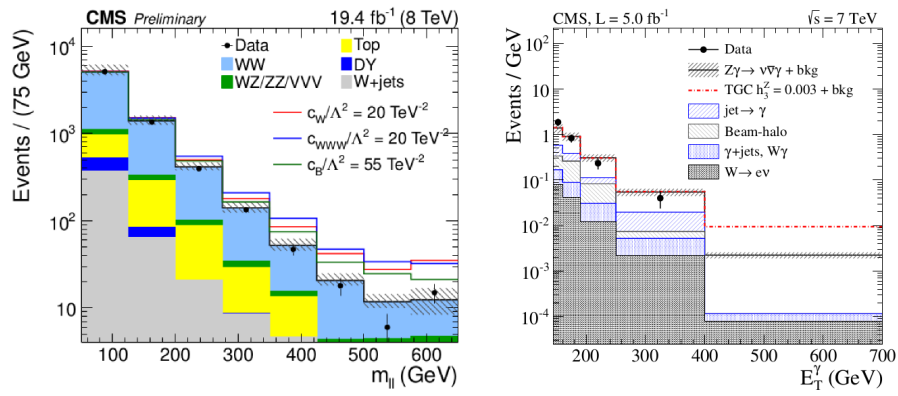
Figure 12: Examples of the potential effects of non-zero TGC constants in $m_{ll}$ spectrum in 8 TeV $WW \to l\nu l\nu$ measurement (left) [28] and $P_T^\gamma$ spectrum in 7 TeV $Z\gamma \to \nu\nu\gamma$ measurement (right) [29].

## 2.5    Measurements in the Past

ATGC parameters of $WW\gamma$ vertex can be probed in $W\gamma$, $WW$, and $WZ$ measurements. Limits on $\Delta\kappa_\gamma$ and $\lambda_\gamma$ constants from different D0 [18], LEP [19], ATLAS [20], [21], [22] and CMS [24], [25], [26], [27] measurements are summarized in Fig. 13.



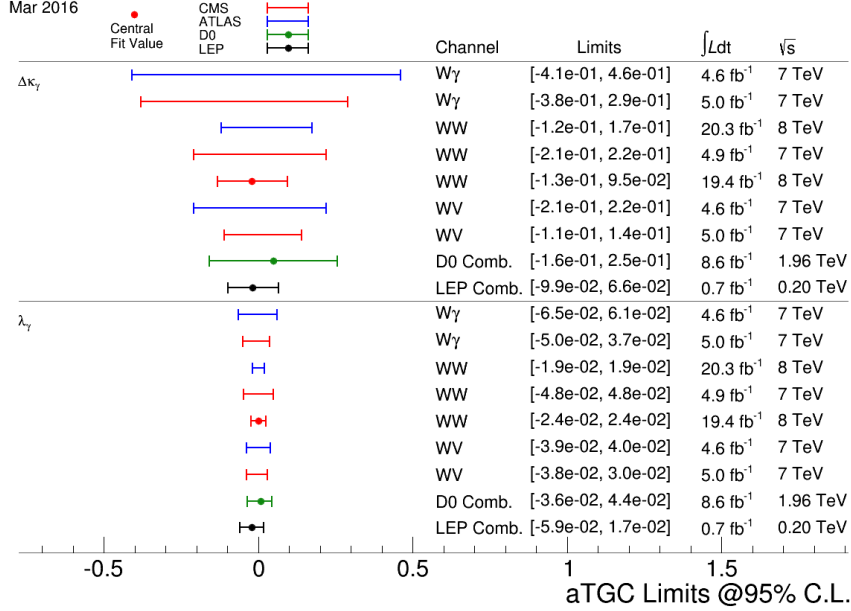| | Channel | Limits | $\int Ldt$ | $\sqrt{s}$ |
|---|---|---|---|---|
| $\Delta\kappa_\gamma$ | W$\gamma$ | [-4.1e-01, 4.6e-01] | 4.6 fb$^{-1}$ | 7 TeV |
| | W$\gamma$ | [-3.8e-01, 2.9e-01] | 5.0 fb$^{-1}$ | 7 TeV |
| | WW | [-1.2e-01, 1.7e-01] | 20.3 fb$^{-1}$ | 8 TeV |
| | WW | [-2.1e-01, 2.2e-01] | 4.9 fb$^{-1}$ | 7 TeV |
| | WW | [-1.3e-01, 9.5e-02] | 19.4 fb$^{-1}$ | 8 TeV |
| | WV | [-2.1e-01, 2.2e-01] | 4.6 fb$^{-1}$ | 7 TeV |
| | WV | [-1.1e-01, 1.4e-01] | 5.0 fb$^{-1}$ | 7 TeV |
| | D0 Comb. | [-1.6e-01, 2.5e-01] | 8.6 fb$^{-1}$ | 1.96 TeV |
| | LEP Comb. | [-9.9e-02, 6.6e-02] | 0.7 fb$^{-1}$ | 0.20 TeV |
| $\lambda_\gamma$ | W$\gamma$ | [-6.5e-02, 6.1e-02] | 4.6 fb$^{-1}$ | 7 TeV |
| | W$\gamma$ | [-5.0e-02, 3.7e-02] | 5.0 fb$^{-1}$ | 7 TeV |
| | WW | [-1.9e-02, 1.9e-02] | 20.3 fb$^{-1}$ | 8 TeV |
| | WW | [-4.8e-02, 4.8e-02] | 4.9 fb$^{-1}$ | 7 TeV |
| | WW | [-2.4e-02, 2.4e-02] | 19.4 fb$^{-1}$ | 8 TeV |
| | WV | [-3.9e-02, 4.0e-02] | 4.6 fb$^{-1}$ | 7 TeV |
| | WV | [-3.8e-02, 3.0e-02] | 5.0 fb$^{-1}$ | 7 TeV |
| | D0 Comb. | [-3.6e-02, 4.4e-02] | 8.6 fb$^{-1}$ | 1.96 TeV |
| | LEP Comb. | [-5.9e-02, 1.7e-02] | 0.7 fb$^{-1}$ | 0.20 TeV |

aTGC Limits @95% C.L.

Figure 13: Summary of limits on the $WW\gamma$ aTGC coupling constants. Figure from [23]

The most recent measurements of $W\gamma$ production were performed by CMS [24] and ATLAS [20] collaborations with $pp$ collisions at $\sqrt{s} = 7$ GeV collected in 2011. The measurements are based on 5 fb$^{-1}$ and 4.6 fb$^{-1}$ of integrated luminosity with CMS and ATLAS respectively. Both collaborations considered two channels: $W\gamma \rightarrow \mu\nu\gamma$ and $W\gamma \rightarrow e\nu\gamma$.

The major source of the background is the fake photon background where hadronic jets are misidentified as photons. Such events originate from $W$+jets process mostly but $Z$+jets and $\bar{t}t$+jets events contribute to this source of the background as well. The second major background for the electron channel is the fake photon background where electron can be misidentified as a photon. Such events are coming from $Z$+jets events. Other sources of backgrounds include real-$\gamma$ backgrounds, fake lepton + real photon and fake lepton + fake photon sources.

The $p_T^\gamma$ spectra of the selected events in data superimposed with selected events in the simulation of the signal and estimated background contribution for the muon and electron channels are shown in Fig. 14 for CMS and in Fig. 15 for ATLAS. Both measurements show a good agreement.

CMS provides measurements of the $P_T^\gamma$ spectrum, the total cross section within the phase spaces of $\Delta R > 0.7$, $P_T^\gamma > 15$ GeV, $P_T^\gamma > 60$ GeV and $P_T^\gamma > 90$ GeV, and limits on aTGC coupling constants.

ATLAS, in addition to the $P_T^\gamma$ spectrum, total cross section and limits, provides the differential cross section and cross section with different number of associated jets. No evidence of a new physics is observed.

In this dissertation we are measuring total and differential $d\sigma/dP_T^\gamma$ cross section however we do not derive limits on aTGC coupling constants. The measurement details and results are
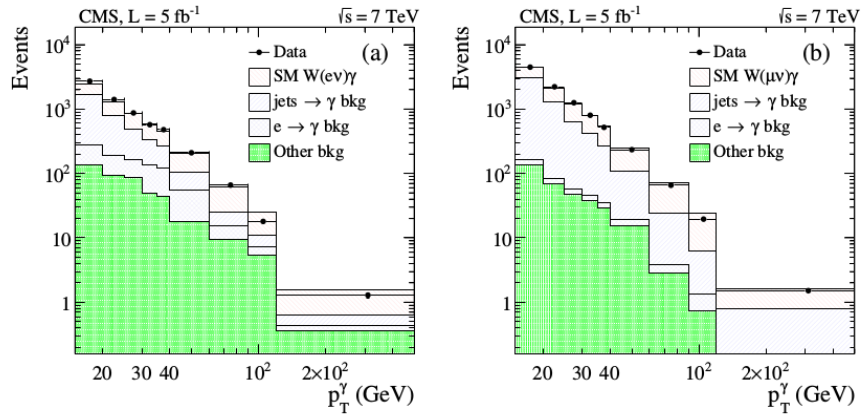
Figure 14: The distribution fo the $p_T^\gamma$ of W$\gamma$ candidates in the analysis of 7 TeV CMS data. Data vs signal MC + background estimates. Left: $W\gamma \to e\nu\gamma$, right: $W\gamma \to \mu\nu\gamma$ [24].
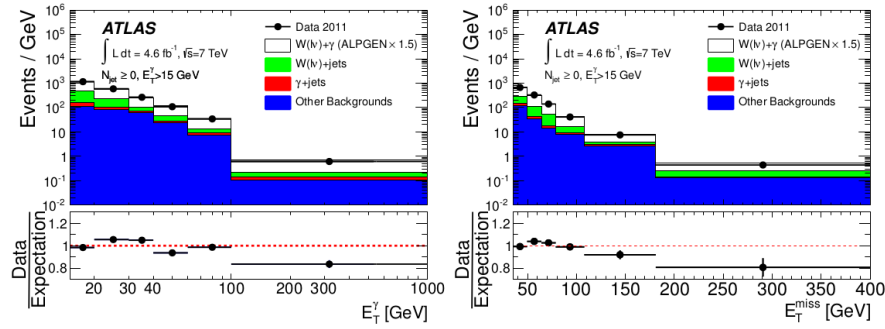


Figure 15: The distribution fo the $p_T^\gamma$ (left) and $E_T^\gamma$ (right) of W$\gamma$ candidates in the analysis of 7 TeV ATLAS data. Data vs signal MC + background estimates [20].

638    available in Chapter 5.

639

# 3 Experimental Setup

## 3.1 Large Hadron Colllider

Large Hadron Collider (LHC) [30], [31], [32] is the last element of the chain of the CERN's accelerator complex (Fig. 16). Before entering LHC, particle beams are going through several stages of the acceleration. Thus, protons are extracted from hydrogen atoms, are accelerated by Linac2 to energies of 5 MeV, then injected into the Proton Synchrotron Booster (PSB) where they reach energies of 1.4 GeV. After that protons are to PS and Super PS (SPS) where they are accelerated to 25 GeV and 450 GeV respectively. Finally, protons enter LHC and are accelerated for 20 minutes to reach their design energies of 7 TeV per beam.

Besides protons, the complex also works with lead ions however in this dissertation we analyze data from proton-proton collisions only and, therefore, are not discussion lead ion collisions in more details.

LHC is the largest particle accelerator ever built: it is about 27 km in circumference. Also LHC re-uses the tunnel built for Large Electron-Positron (LEP) Collider which determines the size of the machine. The large size is necessary to reach design high energies.

Main goals of LHC were to detect the Higgs boson if it existed and to search for evidences of BSM physics which may give a clue on understanding the phenomena which are not described by the SM including dark matter, matter-antimatter asymmetry, gravitational force and others. Six detectors are installed at the LHC to detect particles and perform the relevant measurements. There are general purpose detectors ATLAS and CMS, there is LHCb which specializes of the physics of B-mesons, ALICE which is designed to detect products of heavy ion collisions. In addition, there are two small detectros with very specific tasks: LHCf and TOTEM which are installed close to the ATLAS and CMS interaction points respectively.

No deviations from the SM were found by any of the experiments. The main achivement of the LHC to date is the discovery of the Higgs boson in 2012 by CMS [3] and ATLAS [4] collaborations.

LHC is constructed of eight arcs, each arc corresponds to a sector as shown in Fig. 17. In between there are eight insertions where beams are either collided or injected or dumped or cleaned.

From the other hand, LHC is split on eight octants, each starting from the middle of one sector and ending at the middle of the next one. Thus, each octant includes one full insertion.

Main parameters are summarized in Tab. 2.

Besides a beam energy, the most important quality of the accelerator is ability to produce a large number of interesting collisions which is determined by luminosity. The instantaneous luminosity is determined by the following expression [7]:

$L = f \frac{n_1 n_2}{4\pi\sigma_x\sigma_y}$

where $n_1$ and $n_2$ are numbers of particles in colliding bunches, $f$ is a frequency of collisions, $\sigma_x$ and $\sigma_y$ are beam sizes in horizontal and vertical directions.

To determine the integrated luminosity, one has to integrate the instantaneous luminosity over time:

$L_{int} = \int L dt$

Run periods of LHC in 2010-2012 refer to Run I of the LHC operation. While working on energy of $\sqrt{s} = 7$ TeV (3.5 TeV pae beam), LHC delivered 44.96 pb$^{-1}$ and 6.1 fb$^{-1}$ of data in 2010 and 2011 year respectively. In 2012 the working energy of LHC was $\sqrt{s} = 8$ TeV, and the integrated luminosity was $L_{int} =$23.3 fb$^{-1}$. After a long shutdown, LHC was upgraded for Run II, to operate on $\sqrt{s} = 13$ TeV in 2015 and delivered 4.22 fb$^{-1}$ of data by the end of 2015. In 2016 LHC continues operation on $\sqrt{s} = 13$ TeV and by the end of September the integrated

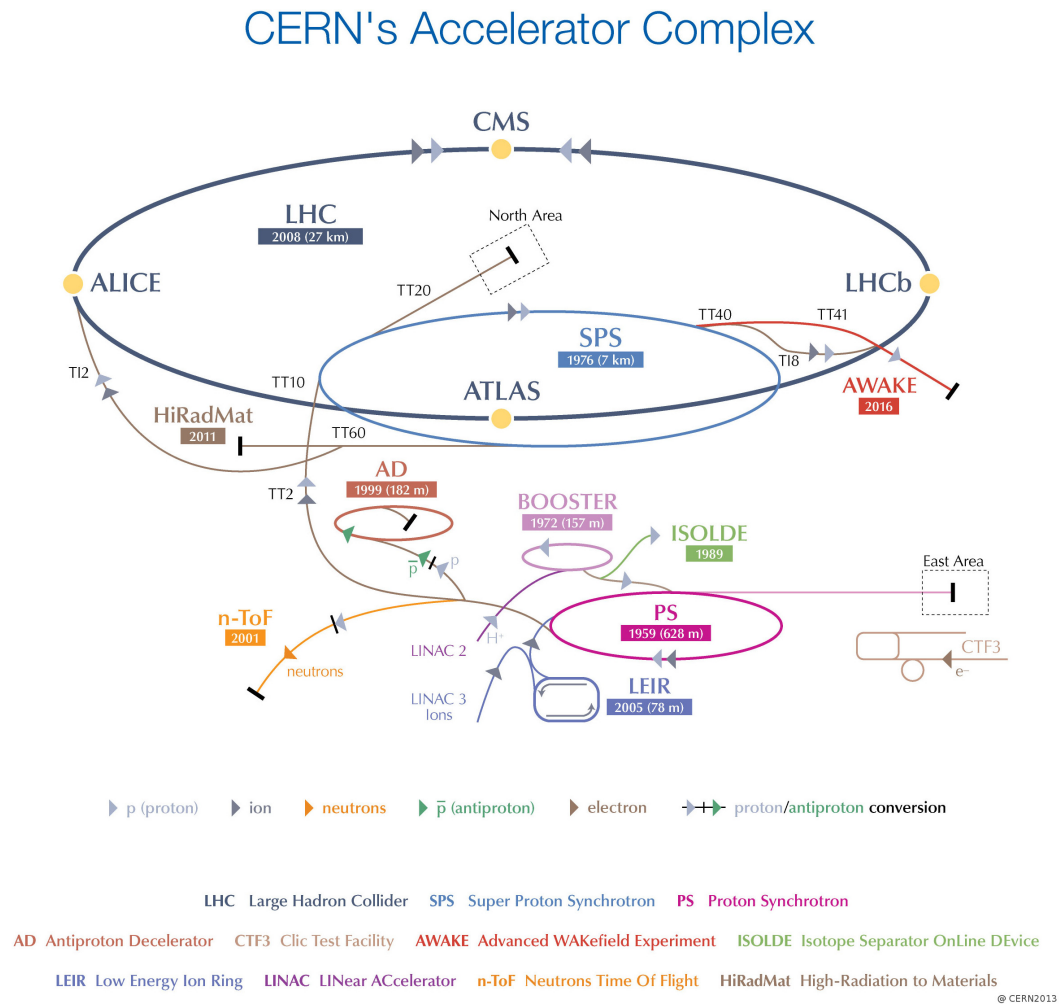luminosity already exceeded a value of 30 fb$^{-1}$ [36].



Figure 16: CERN's accelerator complex. Source of the figure: [33].

Table 2: Main parameters of LHC [30]

| | |
|---|---|
| Circumference | 27 km |
| Dipole operating temperature | 1.9 K |
| Number of magnets | 9593 |
| Number of main dipoles | 1232 |
| Number of main quadrupoles | 392 |
| Number of RF cavities | 8 per beam |
| Nominal energy, protons | 7 TeV |
| Nominal energy, lead ions | 2.76 TeV per nucleon |
| Peak magnetic dipole field | 8.33 T |
| Min. distance between bunches | 7 m |
| Design luminosity | $10^{34}$ cm$^{-2}$ s$^{-1}$ |
| No. of bunches per proton beam | 2808 |
| No. of protons per bunch (at start) | $1.1 \times 1011$ |
| No. of collisions per second | 600 millions |
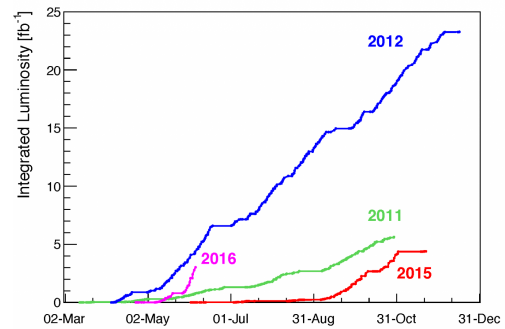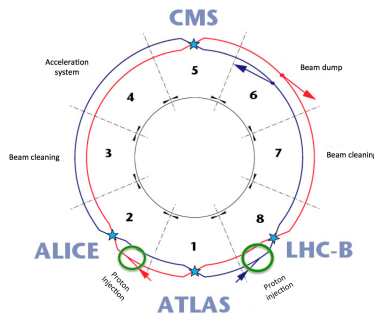


Figure 17: Schematic view of LHC sectors. Source of the figure: [35].

Figure 18: LHC integrated luminosity by year. Source of the figure: [34].

## 3.2 Compact Muon Solenoid

### 3.2.1 Introduction

CMS is a general-purpose detector designed for detecting various particles which are being produced in pp collisions at LHC. Its main feature is a huge magnet to create a magnetic field of 4T to curve charged particles in the tracking system and 2T outside to curve muons in the muon system.

CMS detector is a cylindrically symmetric with a colliding beam as a central axis. The detector consists, from inner to outer layer, of a tracking system, an electromagnetic calorimeter (ECal), a hadronic calorimeter (HCal), a magnet and a muon system. Having the tracking system, ECal and HCal inside of a large solenoid makes the detector "compact". A segment of a CMS slice in $r - \phi$ plane is shown in Fig. 19.

When a heavy particle is produced in a collision, it decays immediately, and we detect its long-living decay products including an electron, a photon, a muon, a neutral hadron or a charged hadron. Depending on the trace left by a particle in different subdetectors we can identify a particle. Electrons and positrons leave curved tracks in the tracking system and then induce showers in the electromagnetic calorimeter (ECal) where they are typically stopped. Photons induce the same electromagnetic showers is ECal however, as neutral particles, they do not leave tracks in the tracking system. Hadrons normally travel through the ECal undisturbed and induce a hadronic shower in the hadronic calorimeter (HCal). Charged and neutral hadrons can be distinguished from each other by checking whether they leave a track in the tracking system or not. Muons are the only particles which are not stopped by the layer of ferrum and leave tracks in the CMS muon system. Neutrinos are not detected by CMS.
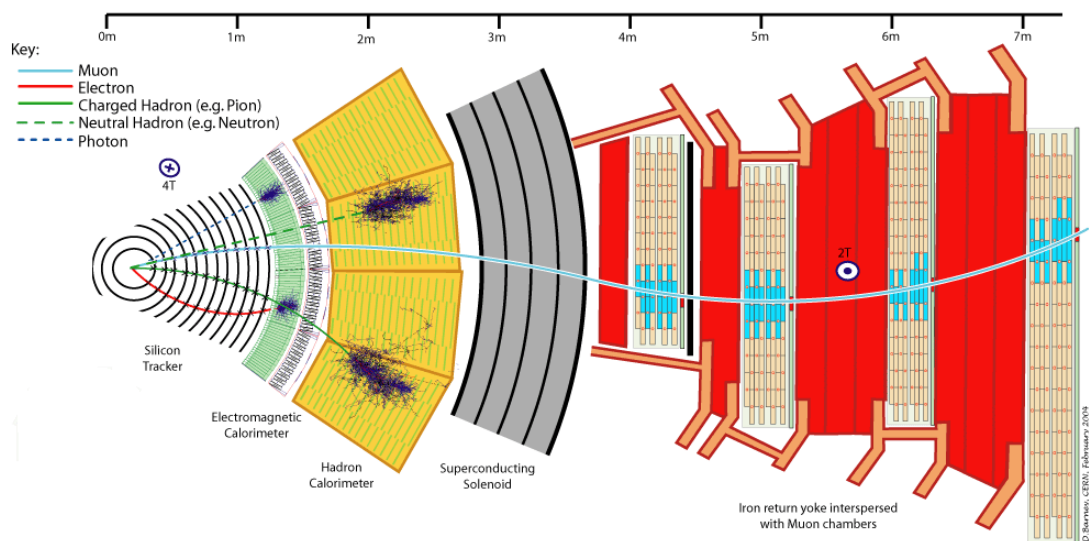


Figure 19: CMS slice.

In $W\gamma$ measurement we have muons and electrons as final state particles. They are both affected by CMS magnetic field allowing the tracking system and the muon system to measure their trajectory parameters and momenta.
In this dissertation we use the information of the primary vertex determined by the tracking system to select our events. Also the tracker provide us the information about electrons trajectories and momenta in the electron channel and distinguishes between electrons and photons.

### 3.2.2  Magnet

A magnetic field in a particle detector is necessary to measure momenta of charged particles by track curvatures. The higher the momentum is, the less a particles's path is affected by the magnetic field. In CMS it is done in the tracking system for all charged particles and in the muon system for muons.

The CMS magnet is placed between layers of HCal and a muon system. It creates a magnetic field of 4T inside the magnet, for the tracking system, and 2T outside the magnet, for the muon system. It is necessary to have stronger field in the tracking system because a density of tracks is much higher there than in the muon system and also the tracking system is much smaller and, therefore, more significant cuvature is necessary to measure the momentum with high precision.

The magnet is made of superconducting wires. An electric current flowing in the wires creates a uniform field inside the solenoid and also provides a magnetic filed of a certain configuration outside the solenoid.

### 3.2.3  Tracking System

The tracking system measures track geometry including particles trajectories and locations of primary and secondary vertices and momenta of charged particles. It needs to disturb particles as little as possible so that they can pass through. Therefore, just a few measurements must be enough to reconstruct the track. The accuracy of a measurement of each hit is 10 $\mu$m.

The tracking system consists of silicon pixels and silicon strips (Fig. 20). Collision tracks start at the center and then cross the layers of the tracking system. Tracks are straight in $r - z$ plane and curved by the magnetic field in the $r - \phi$ plane. The acceptance of the tracker system in $r - z$ plane is geometrically limited by $\eta = 2.5$ ($\eta = -\ln[\tan \theta/2]$, where $\theta$ is a polar angle).

The pixel tracker is the closest subsystem of CMS to the collision point thus it receives the largest particle flux: at 8 cm from the collision point the flux is about 10 million $1/(cm^2 s)$, and the pixel detector with its 65 millions sensors is capable to reconsruct all these tracks. It consists of three layers of cylinders in the barrel with radii of 4 cm, 7 cm and 11 cm and four disks in the endcap, two disks at each side. The tracker is designed in such a way that a single track hits multiple sensors. Then the trajectory is reconstructed based on how much charge is collected on each sensor. This allows us to reach a spacial resolution of 15-20 $\mu$m which is much smaller than a distance between sensors.

The strip tracker is placed right after the pixel tracker and occupies the detector volume up to 130 cm aound the beam axis. The strip tracker consists of four parts: the tracker inner barrel (TIB), the tracker inner disks (TID), the tracker outer barrel (TOB) and the tracker endcap (TEC) as shown in Fig. 20. In the strip tracker there are over 15,000 sensitive modules with a total number of 10 million strips. Each sensitive module consists of a set of sensors, its support structure and readout elements.

### 3.2.4  Electromagnetic Calorimeter

The ECal measures energy of electrons and photons and also measures geometries of their trajectories. Electrons and photons interact with the ECal substance by inducing electromagnetic showers. Traces left by photons and electrons in the ECal are the same. To distinguish between these two particles, it is necessary to perform matching to the track in the tracking system. If there is a track, then there is an electron (or positron). If there is no track, then the particle is a photon.
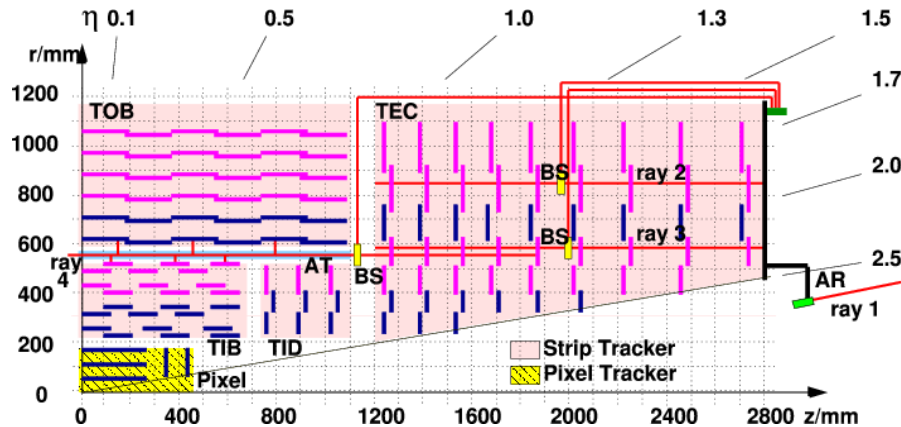
Figure 20: Slice of the CMS tracking system in $r - z$ plane.

The Ecal is a layer between the tracking system and the HCal. It is made of high-density lead tungstate crystals arranged in a barrel section and two endcap sections. The crystals work as scintillators. When electrons and photons pass through it, it produces light proportional to the particle's energy. The scintillated light then is amplified by photomultipliers producing signals on sensitive elements.

It is important for the Ecal to be able to distinguish between high energetic photons and pairs of lower energetic photons e.g. from a $\pi^0$ decay. It is especially difficult in the endcap sections where angle between two photon trajectories is small. Ecal preshowers located in front of the endcaps which have much smaller granularity provide extra spacial precision. Their strips are 2 mm wide compared to 3 cm wide crystals in the main volume of the ECal.

### 3.2.5 Hadron Calorimeter

The HCal is placed right after the ECal and is the last subdetector within the magnet. The HCal measures energies of charged and neutral hadrons. In addition, the HCal determines the track parameters. Match to the tracking system has to be done: if a matching track found, then it is a chagred hadron otherwise it is a neutral hadron.

The HCal consists of alternate layers of absorbers and scintillators. Hadrons hit brass or steel plate of absorber producing secondary particles. When emerge into the scintillator, the particles induce hadronic and electromagnetic showers and emit blue-violet light which is further shifted to the green region and read out by special boxes within the HCal. The secondary hadrons produced during the interaction with the absorber interact with the next absorber producing more showers in the next layers of scintillators and also affect the total enegry deposit. All hadrons must be stopped inside the layers of the HCal.

### 3.2.6 Muon System

Muons pass through the ECal, the HCal and the magnet without interacting. They are the only particles which are registered in the muon system which is placed outside the magnet and which is the largest part of CMS detector.

There are four concentric layers of muon detectors (stations) and iron return yoke between them. Muons induce several hits in the muon stations which are later fitted and matched to the tracking system measurements to provide the best possible resolution in the measurements of all

parameters of the muon's trajectory and momentum.

Overall, there are 1400 muon chambers including 250 drift tubes (DTs), 540 cathode strip chambers (CSCs) and 610 resistive plate chambers (RPCs).

The system of DTs measures positions of muons in the barrel. Each DT chamber is about 2 m by 2.5 m in size. It consists of 12 layers of aluminium which are groups by four. There are up to 60 drift tubes in a layer. The middle group of layers measures $z$-coordinate and two other groups determine the perpendicular coordinate.

Each drift tube is 4 cm in width, is filled with a gas and has a wire inside. When a charged particle passes through the volume, it ionizes atoms and the wire receives an electric charge.
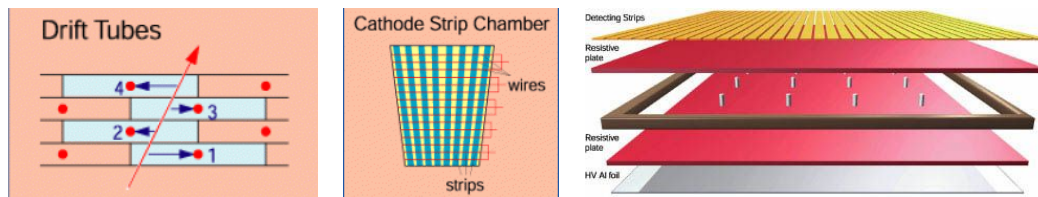
cathode strip chambers resistive plate chambers



Figure 21: Components of the CMS muon system. Left to right: drift tubes, cathode strip chambers (CSCs), resistive plate chambers (RPCs).

### 3.2.7 Triggering and Data Aquisition

Level-I trigger High Level Trigger

### 3.2.8 Event Reconstruction

Where to place particle reconstruction, particle flow algorithm and MET? Check other theses

Acceptance: particles which are too collinear and go to pipe; particles which get curved too strongly

# 4 CMS Tracker Alignment

# 5 W$\gamma$ Cross Section Measurement

Place analysis outline here

# References

[1] Griffiths textbook

[2] website: http://www.isgtw.org/spotlight/go-particle-quest-first-cern-hackfest

[3] CMS Paper about Higgs boson discovery

[4] ATLAS Paper about Higgs boson discovery

[5] website: https://mstwpdf.hepforge.org/

[6] Pich lectures: The Standard Model of Electroweak interactions

[7] PDG

[8] Halzen, Martin "Quarks and leptons"

[9] http://iopscience.iop.org/article/10.1088/0034-4885/70/1/R02

[10] Peskin, Schroeder

[11] Lindsey's thesis (CMS Zg-¿llg, 7 TeV)

[12] website: https://www-d0.fnal.gov/results/publications_talks/thesis/snyder/html/node17.html

[13] website: https://en.wikipedia.org/wiki/Cross_section_%28physics%29

[14] NNLO theory paper

[15] NLO theory paper

[16] aTGC paper

[17] Senka's thesis (CMS Wg-¿munug, 7 TeV)

[18] D0 Combination of W$\gamma$, WW, WZ and VW using 8.6 fb-1 of 2 TeV $p\bar{p}$ collisions Phys.Lett. B718 (2012) 451-459

[19] LEP Combination of WW and single W using 0.7 fb-1 per experiment of $e^+e^-$ collisions at WW pair production energies arXiv:1302.3415

[20] 7TeV Wg ATLAS paper

[21] ATLAS WW using 20.3 fb-1 of 8 TeV pp collisions Submitted to JHEP

[22] ATLAS VW (V=W,Z →jj) using 4.6 fb-1 of 7 TeV pp collisions JHEP 01 (2015) 049

[23] website: https://twiki.cern.ch/twiki/bin/view/CMSPublic/PhysicsResultsSMPaTGC#Figure_1_Limits_on_WW

[24] 7TeV Wg CMS paper

[25] CMS WW using 4.9 fb-1 of 7 TeV pp collisions Eur. Phys. J. C 73 (2013) 2610

[26] CMS WW using 19.4 fb-1 of 8 TeV pp collisions Submitted to EPJC

[27] CMS VW (V=W,Z →jj) using 5.0 fb-1 of 7 TeV pp collisions Eur.Phys.J. C73 (2013) 2283

[28] CMS 8 TeV WW lnulnu

[29] CMS 7 TeV Zg nunug

[30] CERN brochure, http://cds.cern.ch/record/1165534/files/CERN-Brochure-2009-003-Eng.pdf

[31] LHC TDR

[32] website: http://home.cern/topics/large-hadron-collider

[33] website: http://cds.cern.ch/record/1621583/files/

[34] http://home.cern/sites/home.web.cern.ch/files/image/update-for_cern_people/2016/06/intlumirunall_image.png

[35] website: http://cds.cern.ch/journal/CERNBulletin/2014/24/News%20Articles/1706606

[36] website: https://twiki.cern.ch/twiki/bin/view/CMSPublic/LumiPublicResults